Chaos, Solitons and Fractals 210 (2026) 118657

Contents lists available at ScienceDirect

Chaos, Solitons and Fractals

journal homepage: www.elsevier.com/locate/chaos

Targeted adaptive chaos control of regimes and eddy strength in two Lorenz models

Moyan Liu [a,*], Qin Huang [a], Upmanu Lall [a,b]

[a] School of Complex Adaptive Systems & Water Institute, Arizona State University, 1151 S. Forest Ave., Tempe, 85281, AZ, United States
[b] Department of Earth and Environmental Engineering & Columbia Water Center, Columbia University, 2960 Broadway, New York, 10027, NY, United States

ARTICLE INFO

Dataset link: http://github.com/moyan-liu/Lorenz-63-84-control

Keywords:
Lorenz system
Energy-optimal adaptive control
Local Lyapunov exponent

ABSTRACT

We develop an energy-efficient adaptive control framework in two low-order atmospheric dynamical systems, the Lorenz 63 (L63) and Lorenz 84 (L84) models, with multiplicative noise explicitly incorporated. Control is triggered using estimates of the local Lyapunov exponent (LLE), identifying dynamically sensitive states where perturbations are most effective. Once triggered, control amplitudes are determined by solving a constrained optimization problem over a finite forecast horizon that minimizes total control energy while keeping trajectories within prescribed bounds. In L63, regime transitions represent analogs of persistent circulation states, while in L84, large eddy amplitudes serve as surrogates for synoptic-scale moisture transport events such as atmospheric rivers. To account for model uncertainty, we explicitly introduce multiplicative noise and apply control to randomly selected ensemble realizations rather than deterministic trajectories. Despite this stochasticity, effective control is achieved with total energy inputs of only 10^{-3} to 10^{-4} of the system energy. Although highly idealized, these results demonstrate how instability-aware, minimal-energy control strategies can limit extreme states in chaotic systems. In the context of increasing extreme weather under climate change, these results provide a conceptual foundation for the Weather Jiu-Jitsu idea: exploiting the sensitivity of atmospheric dynamics to redirect or defuse high-impact events using small, well-timed perturbations.

1. Introduction

Climate change is intensifying extreme events such as droughts, floods, heat waves, and freezes, causing severe global socio-economic impacts [1]. These effects are further exacerbated by growing populations and increasing economic activity [2]. While current strategies or policies such as decarbonization and the energy transition can reduce greenhouse gas emissions, they do not directly mitigate the immediate risks posed by extreme weather events [3]. Approaches like weather modification and geoengineering require vast amounts of energy and are hindered by significant technical and ethical concerns [4,5]. Meanwhile, scaling aging and inadequate physical, financial, and social infrastructure to enhance resilience remains a formidable challenge [6]. These challenges are complicated by the difficulty in predicting the underlying atmospheric processes that drive extreme weather, particularly persistent atmospheric blocking patterns associated with anomalous jet stream behavior and synoptic scale eddies in the mid-latitudes [7–10]

* Corresponding author.
E-mail address: moyanliu@asu.edu (M. Liu).

https://doi.org/10.1016/j.chaos.2026.118657
Received 30 December 2025; Received in revised form 9 April 2026; Accepted 10 June 2026

We propose an initiative [11] we call "Weather Jiu-Jitsu" to mitigate weather extremes by defusing or redirecting atmospheric circulation trajectories using recurrent nudging with small perturbations that leverages the underlying nonlinear dynamics to amplify the effect of the nudges. For our purposes, we view Lorenz 63 model regime shifts as conceptual analogs of persistent circulation anomalies, while for the Lorenz 84 model we associate high eddy amplitudes with surrogates of synoptic-scale features such as atmospheric rivers. These are not meteorological extremes, but they provide testbeds for asking whether such states can be suppressed or redirected in a controlled setting. This differs from prior chaos control studies, which typically focused on trajectory stabilization without reference to physically motivated extreme states.

The Lorenz 63 (L63) model, emerged from a collaboration between Edward Lorenz and Barry Saltzman and is a notable conceptual example in chaos theory and atmospheric dynamics [12–14]. L63 exhibits sensitive dependence to initial conditions, and given the shape of its attractor, it led to the well-known expression "butterfly effect" [13,15].

The Lorenz 84 (L84) model represents mid-latitude atmospheric circulation under external forcing by the equator to pole temperature gradient and land ocean temperature contrast. The forcing can consider seasonal variability and El Nino Southern Oscillation (ENSO) dynamics [16–18]. It captures certain features of atmospheric behavior that underlie extreme weather, including jet stream oscillations and eddy dynamics [19–21]. These models serve as conceptual testbeds for understanding how weather and climate system can shift into hazardous states and how targeted interventions might delay or deflect such shifts [22–25].

Chaos control techniques have been applied across various fields, including weather and climate systems [26,27]. For example, Control Simulation Experiments (CSE) and Model Predictive Control (MPC), coupled with data assimilation, have been developed to keep the L63 system confined to one wing of the butterfly attractor with control and optimization algorithms, demonstrating successful control outcomes [28–30]. One of the first methods is the Ott–Grebogi–Yorke (OGY) method, which stabilizes chaotic trajectories by applying small perturbations to system parameters when the system naturally approaches an unstable periodic orbit embedded within the chaotic attractor [31,32]. Adaptive targeting methods guide chaotic systems toward desired states using observed trajectories and feedback perturbations [33]. Time-delayed Feedback Control (TDF) stabilizes unstable periodic behavior by applying a correction based on the difference between the system's current state and its own state at a previous time, but relies heavily on past states, which is problematic in high-dimensional, chaotic systems like the atmosphere [34–36]. Sliding Mode Control (SMC) approach has also been applied to the L63 model. It forces the system's state to reach and stay on a predefined surface in the state space, but induces chatting, making it unsuitable for smooth, energy-efficient intervention [37,38]. Reinforcement Learning (RL) offers flexibility but often demands prohibitive computational resources [39].

The past work signals the potential for 'Weather Jiu-Jitsu'. Here, we benchmark an approach that considers an ensemble of trajectory evolution, and the role of "dynamical" noise and thus account for stochastic aspects. Instead of seeking to remove the inherent unpredictability of chaotic systems, the approach works with their nonlinear behavior and dynamically leverages transient sensitivities. These considerations allow a more realistic assessment of an adaptive control strategy than has been done in prior work on idealized models. Instead of applying persistent interventions at every time step, we introduce a strategy that activates control only when a potential regime shift is detected, based on real-time evaluation of local stability in state space, as quantified by local Lyapunov exponents (LLE) [40–42]. Once triggered by a LLE that exceeds a specified threshold, we solve a constrained optimization problem over a specified forecast horizon, to solve for minimal energy perturbations required to direct the system into a desired regime. The strategy is implemented and then re-evaluated at each forward time step, randomly choosing a trajectory from the ensemble generated upon implementation. This approach not only ensures efficient use of control energy resources but also enhances realism by respecting physical limits and maintaining the system's inherent variability.

2. Methods

Our approach is developed and demonstrated on both Lorenz models, though with slightly different objectives. With the L63 model, we consider a goal to keep the trajectories confined to one wing of the butterfly, representing regime control. The intention was to show that our approach is effective, even in the presence of noise. With the L84 model, we consider that strong eddies would represent potentially extreme tropical moisture exports or atmospheric rivers and seek to limit their amplitude by perturbation. This is a more complex forced system, and this experiment gets a little closer to the idea of controlling weather extremes in an idealized environment.

2.1. Lorenz systems

The Lorenz 1963 (L63) model (Lorenz, 1963) was originally developed to represent atmospheric convection and comprises the following three equations:

$$\frac{dx}{dt} = \sigma(y - x), \tag{1}$$

$$\frac{dy}{dt} = x(\rho - z) - y, \tag{2}$$

$$\frac{dz}{dt} = xy - \beta z, \tag{3}$$

Here, x corresponds to the intensity of convective motion, while y and z represent horizontal and vertical temperature differences. The parameters σ, ρ, and β govern the strength of coupling and dissipative processes. The system exhibits a distinctive butterfly-shaped attractor, with trajectories chaotically switching between two "wings", each corresponding to quasi-stable atmospheric

regimes. These regime switches iconify transitions between different climate or weather patterns. The Lorenz63 (L63) model is widely used in chaos control research, allowing benchmarking of control strategies.

We consider the two wings of the attractor as two climate regimes and implement a control strategy that steers the system's trajectory toward a desired regime. This represents a form of anticipatory intervention to avoid undesirable futures, such as the onset of extreme scenarios. The L63 trajectories are simulated using a fourth-order Runge–Kutta scheme with a fixed time step of $\Delta t = 0.01$ and standard parameter values ($\sigma = 10.0,\ \rho = 28.0,\ \beta = 8/3$). For the initial state $(x_0, y_0, z_0) = (8.20747939,\ 10.0860429,\ 23.86324441)$ is adopted from a previous study for comparison [27], as this initial condition exhibits relatively stable behavior during the early stages of evolution. We constrain the active state space to $(x, y, z) \in [(0, 10), (0, 20), (0, 30)]$. For each experiment, we consider a total evolution of 2000 time steps from the initial condition.

The Lorenz 1984 (L84) model is a truncated representation of large-scale atmospheric dynamics at mid-latitudes [16,43,44], with the dynamics defined by the following sets of ordinary differential equations.

$$\frac{dX}{dt} = -Y^2 - Z^2 - aX + aF, \tag{4}$$

$$\frac{dY}{dt} = XY - bXZ - Y + G, \tag{5}$$

$$\frac{dZ}{dt} = bXY + XZ - Z. \tag{6}$$

Here, X represents the strength of the zonal jet stream, while Y and Z describe the amplitudes of the cosine and sine phases of eddies. Nonlinear interaction terms (XY, XZ) represent the amplification of eddies through energy exchange with the jet stream, while $-Y^2$ and $-Z^2$ in the X-equation indicate energy loss from the jet due to this amplification. The terms $-bXZ$ and bXY represent the advection or displacement of the eddies by the mean flow, with $b > 1$ implying faster displacement than amplification. Linear damping terms reflect mechanical and thermal dissipation, with time scaled such that the eddy damping rate is unity and the zonal flow damping rate is scaled by a factor $a < 1$. This non-autonomous model includes two external forcing parameters: the equator-to-pole temperature gradient (F) and the land–ocean temperature contrast (G). These parameters may vary in time to represent seasonal forcing and can also be coupled to ENSO models to reflect atmospheric forcing associated with different ENSO phases [18]. In the present work, both forcings are held fixed, representing a specific seasonal condition.

Synoptic and low-frequency eddies are the primary drivers of ocean-to-land moisture transport in the extratropics with Atmospheric Rivers (ARs) representing concentrated channels of such transport largely formed by synoptic eddies [45,46]. Motivated by this, we implement a control strategy in the L84 model by constraining the combined eddy amplitude, measured as the sum of the absolute values of Y and Z to remain below a prescribed threshold, as described in Section 3.4. This approach aims to mimic the suppression of excessive eddy activity that may lead to ARs. The L84 trajectories are also simulated with a fourth-order Runge–Kutta scheme with a fixed time step of $\Delta t = 0.01$, employing standard parameter values ($F = 8.0,\ a = 0.25,\ b = 4.0,\ G = 1.0$).

2.2. Local Lyapunov exponents

The solution space of Lorenz models can be considered as a nonlinear dynamical map, where the future state depends in a complex and sensitive way on the current one. We develop a surrogate dynamical map to approximate both the L63 and L84 dynamics (see Supporting Information Text S1). The surrogate reduces the computational cost relative to full Runge–Kutta 4th order (RK) integration while preserving the dominant dynamical behaviors. Conceptually, it functions as a lightweight forecast model, which parallels our long-term goal of applying adaptive control to real weather prediction systems.

Forecasts of chaotic systems are characterized by the exponential divergence of nearby trajectories. The rate of this divergence is quantified by the Lyapunov Exponent (LE) [47,48]. A positive LE indicates that nearby trajectories will diverge with time, while 0 or negative values reflect stability. We focus on the local Lyapunov exponent (LLE), which evaluates divergence rates over short time intervals and localized regions of the state space, enabling the detection of transient instability and regime shifts in real time [40,49,50]. If the LLE is positive an appropriately placed perturbation may amplify in the desired direction, while if the LLE is 0 or negative, changing the trajectory by perturbation may require substantial energy input. Further, in the positive LLE situation, even after perturbation the trajectories are wont to diverge so tracking the actual trajectory that emerges over an operational forecast and control horizon and refocusing it becomes necessary.

Metrics such as the finite-size Lyapunov exponent (FSLE) and finite-time Lyapunov exponent (FTLE) have been developed to quantify predictability over finite spatial scales or finite durations respectively [51,52]. These metrics are useful when extending the analysis to higher-dimensional systems with spatio-temporal dynamics.

To assess local instability at each time step, we compute the local Lyapunov exponent (LLE) using the Jacobian matrix of the surrogate system represented by the map. This metric characterizes the local linear instability of the system to infinitesimal perturbations. For a dynamical system of the form $\dot{\mathbf{x}} = f(\mathbf{x}(t))$, where $\mathbf{x} \in \mathbb{R}^n$ is the state vector and f is a nonlinear vector field, the Jacobian matrix $J(\mathbf{x})$ is defined as

$$J(\mathbf{x}) = \frac{\partial f}{\partial \mathbf{x}} = \begin{bmatrix} \frac{\partial f_1}{\partial x_1} & \cdots & \frac{\partial f_1}{\partial x_n} \\ \vdots & \ddots & \vdots \\ \frac{\partial f_n}{\partial x_1} & \cdots & \frac{\partial f_n}{\partial x_n} \end{bmatrix}. \tag{7}$$

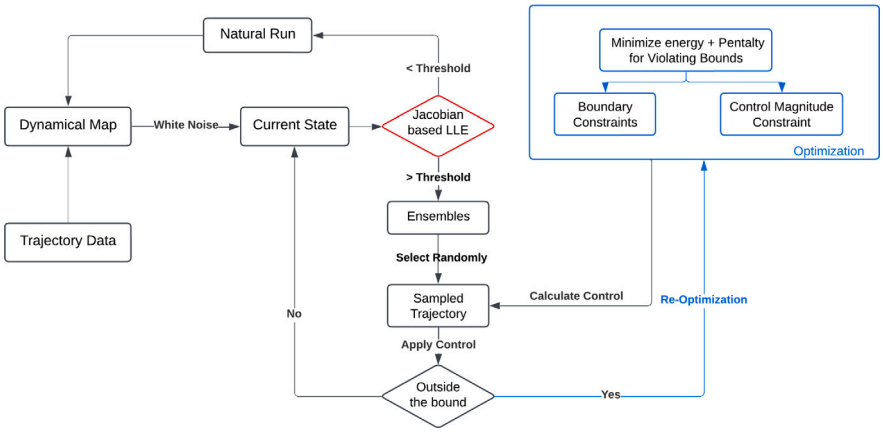

Fig. 1. Workflow of control framework. Diamond-shaped boxes represent decision points (or questions), while rectangular boxes indicate actions taken.

We evaluate the instantaneous LLE as a metric for local, short-term sensitivity in the Lorenz system. This quantity is governed by the Eulerian rate-of-strain tensor, given by the symmetric part of the Jacobian,

$$S(\mathbf{x}) = \frac{1}{2}\left(J(\mathbf{x}) + J(\mathbf{x})^{\mathrm{T}}\right). \tag{8}$$

At any given instant, the instantaneous LLE is defined by the largest eigenvalue of $S(\mathbf{x})$,

$$\lambda(\mathbf{x}) = \max\left(\mathrm{eigvals}\left(S(\mathbf{x})\right)\right). \tag{9}$$

2.3. Experiment design

The overall workflow (Fig. 1) follows a structured pipeline consisting of state evolution, instability detection, control optimization, and performance assessment.

We first calculate the LLE of the current state. If the LLE remains below a prescribed threshold, no control is exercised. If the LLE goes above the threshold, the control mechanism is triggered. Each time we control, we generate 50 ensemble members adding Gaussian noise, in order to account for uncertainty in both the system evolution and model predictions. From this ensemble, one member is randomly selected as the control target, and the optimization algorithm for control is applied to it. The optimization seeks to minimize the total energy used for control by selecting a bounded perturbation sequence. The trajectory evolved using the sequence, with a random member of the ensemble picked at every time step, and the LLE criteria checked at every step to decide if the optimization should be performed again.

The white-noise amplitude is made proportional to the magnitude of the current state variables, to account for model imperfections and observational uncertainty. Before applying the control, the resulting trajectory is re-evaluated over a short verification horizon. If the trajectory remains within the specified bounds, the control is accepted and applied. If not, the optimization is repeated up to a maximum number of attempts. If no successful control is found, the one with the lowest cumulative constraint violation is applied as a fallback.

2.4. Optimized control on triggering

The control objective is to minimize the total energy applied via perturbations over the control horizon, typically specified as $T = 10$ time steps. The decision variables are the magnitudes of the state perturbations, defined as the Euclidean norm of the perturbation vector $\delta\mathbf{X}_t = (dx, dy, dz)$.

$$\min_{\delta\mathbf{X}_t} \sum_{t=1}^{T} \left(u_t^2 + \alpha \sum_{j=1}^{3} \mathrm{penalty}_{t,j}(\mathbf{X}_t) \right), \tag{10}$$

where

$$u_t = \|\delta\mathbf{X}_t\|_2, \quad t = 1, \ldots, T. \tag{11}$$

For each time step over the control horizon, a random noise term is injected into the model dynamics with magnitude m. To maintain feasibility, the magnitude of the control input is constrained by a maximum allowable perturbation $D_{\max}$ to prevent unrealistically large interventions. The controlled system evolves according to

$$\mathbf{X}_t = f(\mathbf{X}_{t-1}, u_t) + \varepsilon_t, \qquad \varepsilon_t \sim \mathcal{N}\left(0,\, m \cdot |\mathbf{X}_{t-1}|\right), \tag{12}$$

subject to

$$u_t \leq D_{\max}, \quad t = 1, \ldots, T. \tag{13}$$

The resulting trajectory is required to remain within prescribed bounds to effect control. A penalty is applied for each component of the forecasted state that violates its respective safety range, defined by lower and upper limits l_j and h_j. The penalty weight α governs the trade-off between minimizing control effort and enforcing state constraints. We adopt a linear penalty for constraint violations as a relaxation of the constrained optimization problem, allowing controlled violations of the bounds when strict enforcement would require disproportionately large control energy. The penalty function is defined as

$$\text{penalty}_{t,j} = \begin{cases} l_j - x_{t,j}, & \text{if } x_{t,j} < l_j, \\ x_{t,j} - h_j, & \text{if } x_{t,j} > h_j, \\ 0, & \text{otherwise.} \end{cases} \tag{14}$$

This model is solved using the Sequential Least Squares Programming (SLSQP) optimization algorithm [53]. If needed, the re-optimization is executed up to 8 times at a particular time step using the same noise realization. The overall control framework is identical for both the L63 and L84 systems, although the specific parameter values and thresholds differ between the two models. To assess performance, we evaluate the ratio of control energy to total system energy at each time step, providing a measure of the relative energy expenditure of the control intervention. This ratio is defined as

$$\frac{E_{\text{control}}}{E_{\text{total}}} = \frac{u_t^2}{X_t^2 + Y_t^2 + Z_t^2}, \tag{15}$$

where (X_t, Y_t, Z_t) denotes the system state at the moment of control application. This metric provides a quantitative measure of the efficiency and subtlety of the intervention.

3. Results

We present the application of the schema from the previous section to the L63 and L84 experiments.

3.1. Control of L63 effectively suppresses regime transitions

The proposed control framework confines the L63 trajectory to one wing of the attractor, eliminating transitions between regimes. In the uncontrolled simulation, the system frequently switches between the two wings of the Lorenz attractor, reflecting the inherent chaotic nature of the model. When the control strategy is applied, these transitions are suppressed, and the trajectory remains on a single wing for the duration of the 2000-step simulation (Figs. 2 (a, b) and Figure S3). Control interventions were triggered at only 201 time steps, with most perturbation magnitudes below 0.5. The control energy, measured as a percentage of total system energy, remained under 0.03% in nearly all cases (Figs. 2 (c, d)). These results highlight the controller's ability to maintain the system in a stable regime using minimal and optimized interventions.

3.2. Infeasible control given initial condition scenario

To evaluate the dependence on initial condition, the initial state $[1, 1, 1]$ was chosen because it lies near the boundary separating the two wings of the L63 attractor wings, a location known to be highly sensitive to perturbations. In this case, the natural trajectory exhibits rapid transitions between regimes, making stabilization intrinsically difficult (Fig. 3). In this early phase, the controller struggles to suppress this instability (high LLE) because the effective control is infeasible within the energy constraints, and therefore no control action is applied. Control was triggered 214 times (compared to 201 in the baseline), with early perturbations often exceeding a magnitude of 0.8. The energy input also rose with control energy exceeding 0.5% of total system energy in the early time steps. However, once the system settled near one wing, both the magnitude and frequency of interventions decreased substantially. This behavior illustrates the importance of an early state selection for intervention, since it is difficult to intervene close to regime transitions where the LLEs are very high.

3.3. LLE thresholds trade-off between timeliness and efficiency

Tuning the LLE threshold allows for better balance between early intervention and total energy cost. By varying the threshold used to trigger control, we assess the sensitivity of the control strategy to instability detection (Supporting Information Figure S4). High thresholds delay intervention, allowing the system to evolve further into chaotic regimes before correction. While this reduces the number of control actions, it also results in higher energy usage due to stronger perturbations being required. In contrast, very low thresholds (e.g., −1.0) lead to frequent interventions. Across tested values, threshold at 0 provided the best balance, stabilizing the system efficiently while minimizing energy costs (Figure S4). These results suggest that optimizing the LLE threshold is useful for deploying energy-efficient control strategies in chaotic systems.

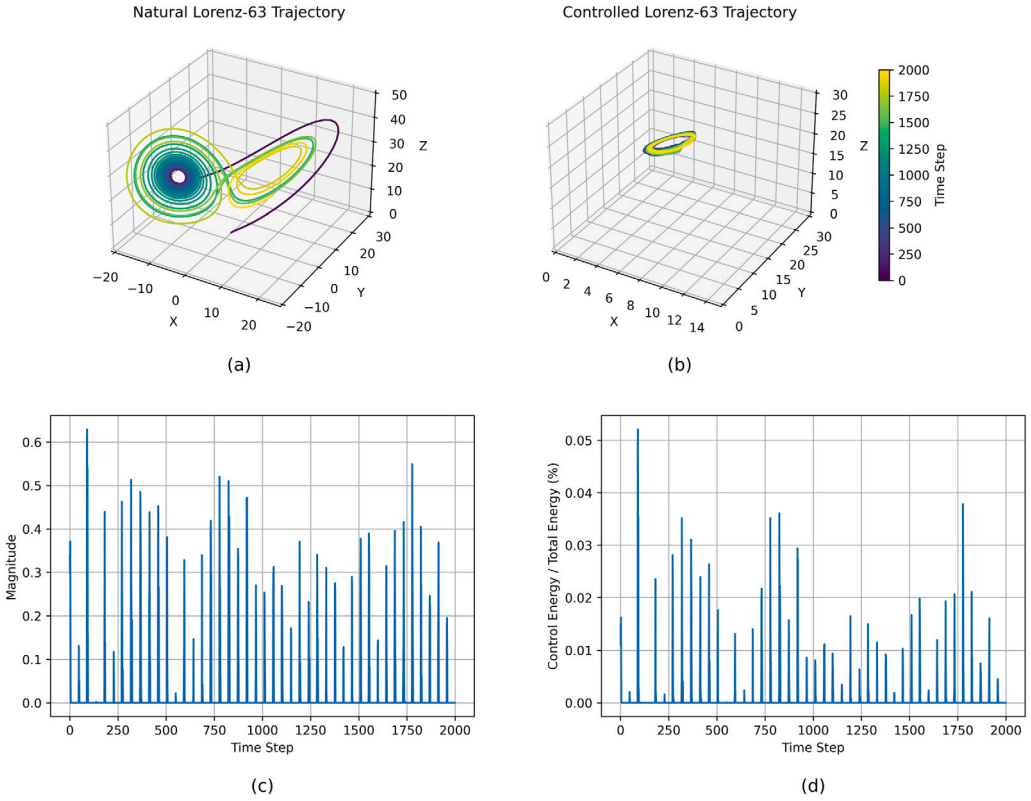

Fig. 2. Comparison of natural (a) and controlled (b) L63 trajectories. (c) shows the magnitude of perturbations applied at each step, and (d) displays the ratio of control energy to total system energy over time. Note that (b) is a zoomed in version of (a) - the axes scales are not the same.

3.4. Control of eddies in L84

To determine an appropriate leading indicator for triggering control of eddy energy in the Lorenz–84 (L84) model, we analyze the relationship between eddy amplitude, quantified by $|Y| + |Z|$, and the local Lyapunov exponent (LLE) over 10,000 time steps. As shown in Supporting Information Sections S5 and S6, both quantities exhibit strong temporal fluctuations, with elevated LLE values generally coinciding with peaks in $|Y| + |Z|$. This behavior reflects increased dynamical instability and chaoticity when eddy amplitudes become large, consistent with physical intuition. We therefore select the 90th percentile of $|Y| + |Z|$ as a threshold indicating high eddy activity, corresponding to an LLE value of approximately 2.4. In this setting, our objective is to intervene over short time windows to suppress the growth of extreme eddies, in contrast to the Lorenz–63 case where continuous-time control of the system state was employed.

To assess the effectiveness of the control strategy applied to the L84 model, we compare the natural and controlled system trajectories (Fig. 4). The natural trajectory exhibits pronounced variability and frequent excursions beyond the threshold radius $|Y| + |Z| > 2.4$, indicating highly active eddies. In contrast, the controlled trajectory remains well confined within the inner region of the attractor. Supporting Information Section S8 quantifies the associated control effort, demonstrating that the control energy remains below 2% of the total system energy for the majority of the simulation, with only occasional peaks when the system approaches transitions toward unstable behavior. These results indicate that the proposed control strategy effectively limits extreme eddy activity in the L84 system.

3.5. Computational cost and control performance

Each optimization step completes in under 0.1 s, enabling potential real-time or online applications. The selective control strategy relies on solving a constrained optimization problem at each intervention step using the SLSQP algorithm. Across 2000 time steps, the average runtime per optimization was approximately 0.09 s. For the L63 simulation, this resulted in a total runtime of ~80 s. In the L84 case, runtime increased to ~25 s due to the rare extreme scenario events. All simulations were executed in Python 3.11.3 on a system with an i386 architecture, 2 physical cores (4 logical), using a single-threaded configuration. These results indicate that the control method is computationally feasible for the idealized models, and could be further accelerated through parallelization or compiled implementations.

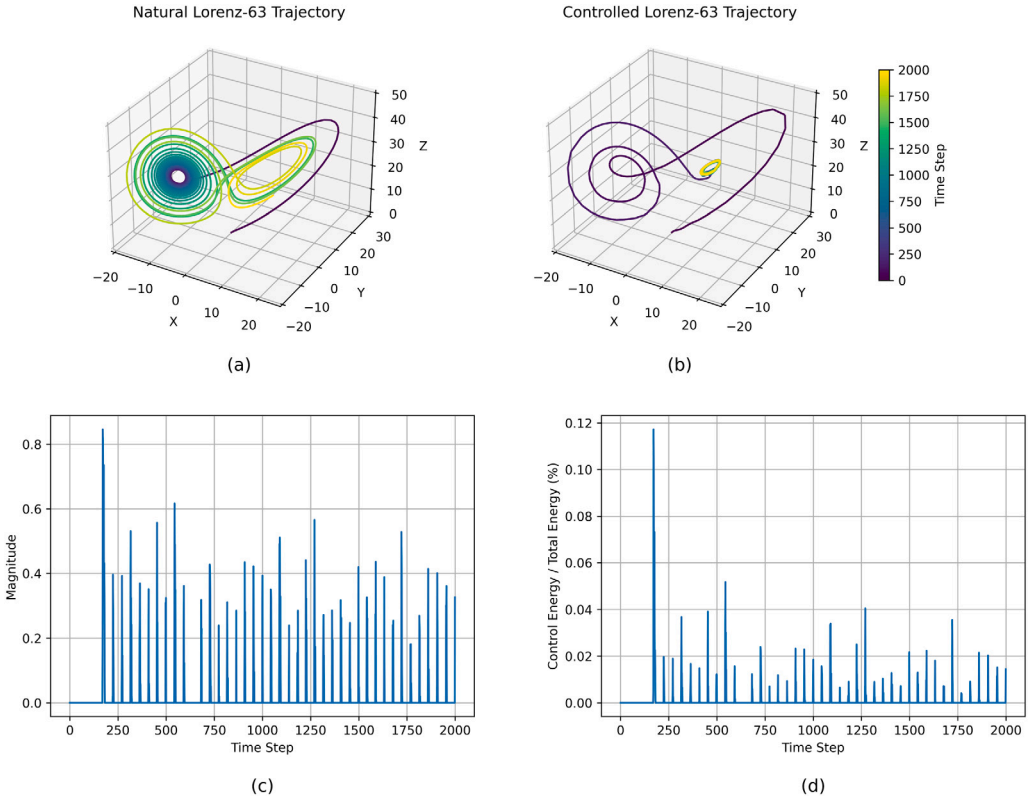

Fig. 3. Comparison of natural (a) and controlled (b) L63 trajectories under an unstable initial condition. (c) shows the magnitude of perturbations applied at each step, and (d) displays the ratio of control energy to total system energy over time.

To further quantify the efficiency of the LLE-triggered strategy, we compare it against a naive geometric baseline that applies the same optimization method but activates control based solely on state thresholds, without using instability information. The baseline requires higher control energy and exhibits reduced effectiveness in maintaining the desired regime compared to the LLE-triggered strategy (Tables S1–S2 and Figures S7–S9). To assess robustness beyond individual illustrative trajectories, we additionally quantified control success rates across multiple initial conditions. For each model, a set of randomly sampled initial states was generated using different parameter settings. Control success was defined in terms of sustained regime confinement for L63 and suppression of large eddy amplitudes for L84. Statistical summaries of success rates and associated control energy are reported in the Supporting Information (Table S3). These results demonstrate that the proposed LLE triggered strategy achieves high success rates while maintaining low average control effort, supporting both the computational efficiency and practical robustness of the framework.

4. Discussion and conclusions

Our intent was to explore whether a practically motivated approach to simulation and adaptive control could be effective for two target idealized atmospheric models, with slightly different goals. We were able to demonstrate computational and operational feasibility and explore conditions that are challenging and sensitivity to parameter choices. A significant finding is that the energy required for achieving control is typically very small compared to the system's energy. This finding is tempered by the demonstration that the success of control depends on the initial condition. Control of the trajectories may not be possible in situations where the LLE's are very high and the system is near a regime transition. This observation is not surprising, but it speaks to the need to appropriately choose the LLE threshold as a trigger and to the time needed to initiate control prior to the event of concern.

Japanese researchers are currently working with Japan's Moonshot 8 project aiming to achieve controlling and modifying weather by 2050 [54]. Their approach applies Control Simulation Experiments (CSE) and Model Predictive Control (MPC) to constrain L63 dynamics to one wing of the attractor, emphasizing data assimilation to select stable ensemble trajectories for potential real-world implementation.

In the present work, we explore a complementary perspective focused on event-driven, targeted control under state uncertainty in a low-order setting. Rather than addressing generic trajectory stabilization, we target model defined extreme states (regime transitions in L63 and large eddy amplitudes in L84) linking the control objective to conceptually relevant meteorological

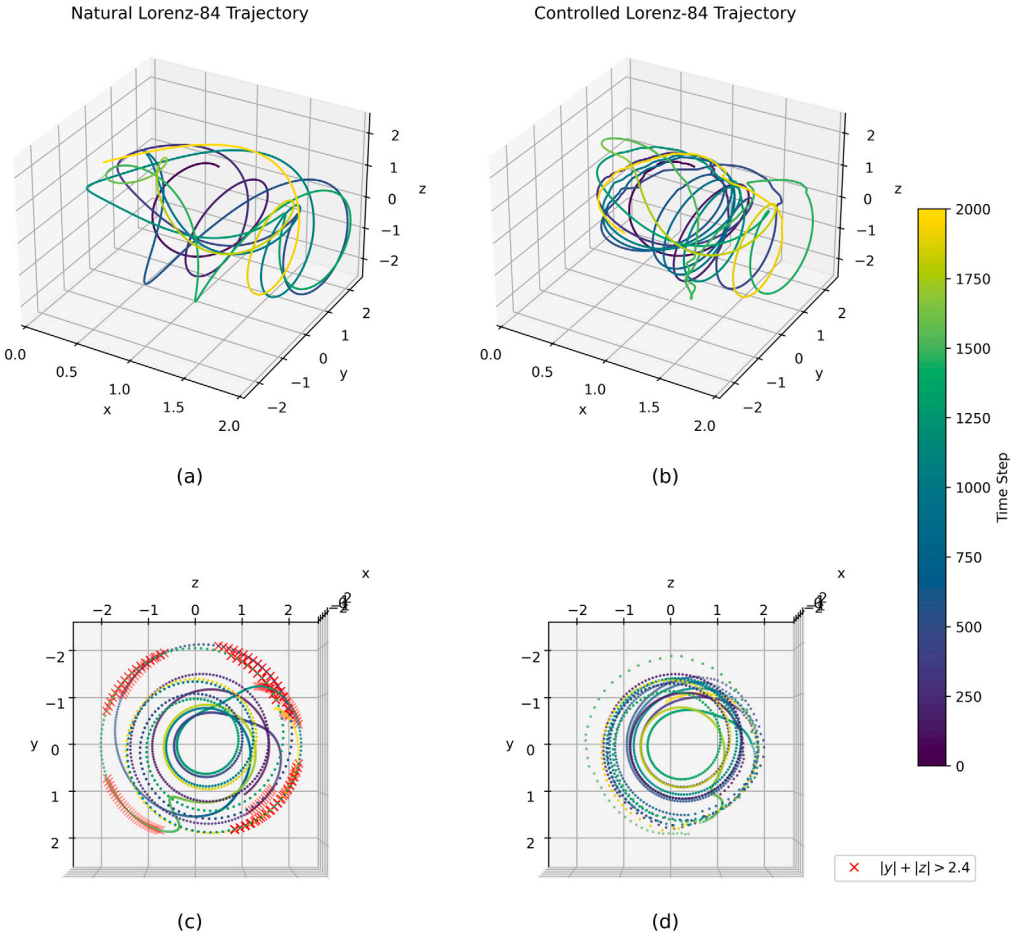

Fig. 4. Colored trajectory plots of L84 under natural (a, c) and controlled (b, d) conditions from two different viewing angles. Red dots in (c) and (d) indicate time steps where the combined eddy amplitude satisfies $|Y| + |Z| > 2.4$. (For interpretation of the references to color in this figure legend, the reader is referred to the web version of this article.)

phenomena. Uncertainty in both model dynamics and observations is represented through stochastic perturbations and ensemble forecasting, allowing us to assess control robustness under realistic variability. Control is activated selectively when local instability is detected, and the associated optimization simultaneously minimizes control energy, consistent with the philosophy of "Weather Jiu-Jitsu": subtly redirecting, rather than resisting, chaotic dynamics. While data assimilation is not explicitly implemented here, the proposed framework is naturally compatible with DA based state estimation and is intended as a complementary building block for future hybrid approaches. This perspective is supported by recent theory linking data assimilation and control through chaos synchronization, whereby observational updates introduce correction terms that are mathematically analogous to control inputs [55]. Ultimately, we believe that hybridization of instability diagnostics, data assimilation, and targeted optimization offers the most promising path forward for practical control of complex geophysical systems.

To extend this concept to operational weather systems, we plan to integrate our control framework with recent advances in data-driven forecasting and real-time decision-making. Our ongoing work focuses on combining deep learning weather foundation models, such as Aurora, AIFS and Pangu [56–58], extending the approach demonstrated here to a dramatically higher dimensional space. While the conceptual logic would be similar, the decision process must now address where and when to intervene, targeting specific spatio-temporal attributes of concern. Of course, these are still thought experiments, motivated by the very high potential value of disaster reduction, and one also needs to identify practical mechanisms for creating the perturbations. Some ideas in that regard are discussed in [11]. These are challenging problems, and we invite collaborations on all aspects of developing the ideas.

CRediT authorship contribution statement

Moyan Liu: Writing – review & editing, Writing – original draft, Visualization, Validation, Methodology, Investigation, Formal analysis, Conceptualization. **Qin Huang:** Writing – review & editing, Methodology, Conceptualization. **Upmanu Lall:** Writing – review & editing, Supervision, Resources, Methodology, Conceptualization.

Declaration of competing interest

The authors declare that they have no known competing financial interests or personal relationships that could have appeared to influence the work reported in this paper.

Appendix A. Supplementary data

Supplementary material related to this article can be found online at https://doi.org/10.1016/j.chaos.2026.118657.

Data availability

No new data were used in this study. All results are based on a theoretical model described in the manuscript. Therefore, no data or software are archived. The code used to run the simulations and produce the figures is available in our GitHub repository: http://github.com/moyan-liu/Lorenz-63-84-control.

References

[1] Robinson A, Lehmann J, Barriopedro D, Rahmstorf S, Coumou D. Increasing heat and rainfall extremes now far outside the historical climate. Npj Clim Atmospheric Sci 2021;4(1):45. http://dx.doi.org/10.1038/s41612-021-00202-w, URL https://www.nature.com/articles/s41612-021-00202-w.

[2] Mario E, Raffaele L, Onofrio C, Maria C-SJ, Valentina B, Vincenzo G, Shao C, Giovanni S. Coupling heat wave and wildfire occurrence across multiple ecoregions within a eurasia longitudinal gradient. Sci Total Environ 2024;912:169269. http://dx.doi.org/10.1016/j.scitotenv.2023.169269, URL https://www.sciencedirect.com/science/article/pii/S0048969723078993.

[3] Zhao Y. CCUS: A panacea or a placebo in the fight against climate change? Green Energy & Environ 2025;10(2):239–43. http://dx.doi.org/10.1016/j.gee.2024.10.001, URL https://www.sciencedirect.com/science/article/pii/S2468025724002826.

[4] Sugiyama M, Asayama S, Kosugi T, Ishii A, Watanabe S. Public attitude toward solar radiation modification: results of a two-scenario online survey on perception in four Asia–Pacific countries. Sustain Sci 2025;20(2):423–38. http://dx.doi.org/10.1007/s11625-024-01520-7.

[5] Yeh ET. Global geographies of weather modification in an era of climate change. Ann Am Assoc Geogr 2025;115(4):949–67. http://dx.doi.org/10.1080/24694452.2025.2450200, URL https://www.tandfonline.com/doi/full/10.1080/24694452.2025.2450200.

[6] Hwang J, Lall U. Increasing dam failure risk in the USA due to compound rainfall clusters as climate changes. Npj Nat Hazards 2024;1(1):27. http://dx.doi.org/10.1038/s44304-024-00027-6, URL https://www.nature.com/articles/s44304-024-00027-6.

[7] Nabizadeh E, Hassanzadeh P, Yang D, Barnes EA. Size of the atmospheric blocking events: Scaling law and response to climate change. Geophys Res Lett 2019;46(22):13488–99. http://dx.doi.org/10.1029/2019GL084863, URL https://agupubs.onlinelibrary.wiley.com/doi/10.1029/2019GL084863.

[8] Han J, Singh VP. Impacts of rossby wave packets and atmospheric rivers on meteorological drought in the continental United States. Water Resour Res 2021;57(12). http://dx.doi.org/10.1029/2021WR029966, e2021WR029966. URL https://agupubs.onlinelibrary.wiley.com/doi/10.1029/2021WR029966.

[9] Aemisegger F, Vogel R, Graf P, Dahinden F, Villiger L, Jansen F, Bony S, Stevens B, Wernli H. How rossby wave breaking modulates the water cycle in the north atlantic trade wind region. Weather Clim Dyn 2021;2(1):281–309. http://dx.doi.org/10.5194/wcd-2-281-2021, URL https://wcd.copernicus.org/articles/2/281/2021/.

[10] Kim J-H, Nam S-H, Kim M-K, Serrano-Notivoli R, Tejedor E. The 2022 record-high heat waves over southwestern europe and their underlying mechanism. Weather Clim Extrem 2024;46:100729. http://dx.doi.org/10.1016/j.wace.2024.100729, URL https://www.sciencedirect.com/science/article/pii/S2212094724000902.

[11] Huang Q, Liu M, Lall U. Weather jiu-jitsu: Climate adaptation for the 21st century. 2025, URL https://arxiv.org/abs/2508.09376 arXiv:2508.09376.

[12] Saltzman B. On the maintenance of the large-scale quasi-permanent disturbances in the atmosphere. Tellus A: Dyn Meteorol Ocean 1959;11(4):425–31. http://dx.doi.org/10.3402/tellusa.v11i4.9329, URL https://account.a.tellusjournals.se/index.php/su-j-tadmo/article/view/3553.

[13] Lorenz EN. Deterministic nonperiodic flow. "Journal Atmospheric Sciences" 1963;20(2):130–41. http://dx.doi.org/10.1175/1520-0469(1963)020<0130:DNF>2.0.CO;2.

[14] Saltsman B. Equations governing the energetics of the larger scales of atmospheric turbulence in the domain of wave number. J. Atmos. Sci. 1957;14(6):513–23. http://dx.doi.org/10.1175/1520-0469(1957)014<0513:EGTEOT>2.0.CO;2.

[15] Glasner E, Weiss B. Sensitive dependence on initial conditions. Nonlinearity 1993;6(6):1067. http://dx.doi.org/10.1088/0951-7715/6/6/014.

[16] Lorenz EN. Irregularity: a fundamentd property of the atmosphere. Tellus A: Dyn Meteorol Ocean 1984;36(2):98. http://dx.doi.org/10.3402/tellusa.v36i2.11473, URL https://a.tellusjournals.se/article/10.3402/tellusa.v36i2.11473/.

[17] Broer H, Simó C, Vitolo R. Bifurcations and strange attractors in the lorenz-84 climate model with seasonal forcing. Nonlinearity 2002;15(4):1205. http://dx.doi.org/10.1088/0951-7715/15/4/312.

[18] Karamperidou C, Cioffi F, Lall U. Surface temperature gradients as diagnostic indicators of midlatitude circulation dynamics. "Journal Climate" 2012;25(12):4154–71. http://dx.doi.org/10.1175/JCLI-D-11-00067.1, URL https://journals.ametsoc.org/view/journals/clim/25/12/jcli-d-11-00067.1.xml.

[19] Madonna E, Li C, Grams CM, Woollings T. The link between eddy-driven jet variability and weather regimes in the north atlantic-European sector. Q J R Meteorol Soc 2017;143(708):2960–72. http://dx.doi.org/10.1002/qj.3155, URL https://rmets.onlinelibrary.wiley.com/doi/10.1002/qj.3155.

[20] Lorenz EN. Can chaos and intransitivity lead to interannual variability? Tellus A 1990;42(3):378–89. http://dx.doi.org/10.1034/j.1600-0870.1990.t01-2-00005.x, URL https://onlinelibrary.wiley.com/doi/abs/10.1034/j.1600-0870.1990.t01-2-00005.x.

[21] Faranda D, Sato Y, Messori G, Moloney NR, Yiou P. Minimal dynamical systems model of the northern hemisphere jet stream via embedding of climate data. Earth Syst Dyn 2019;10(3):555–67. http://dx.doi.org/10.5194/esd-10-555-2019, URL https://esd.copernicus.org/articles/10/555/2019/.

[22] Palmer TN. Predictability of weather and climate: from theory to practice. In: Palmer T, Hagedorn R, editors. Predictability of weather and climate. Cambridge: Cambridge University Press; 2006, p. 1–29. http://dx.doi.org/10.1017/CBO9780511803260.002.

[23] MacMynowski DG. Controlling chaos in el Niño. In: Proceedings of the 2010 American control conference. 2010, p. 4090–4. http://dx.doi.org/10.1109/ACC.2010.5530629.

[24] Shen B-W, Pielke RA, Zeng X, Baik J-J, Faghih-Naini S, Cui J, Atlas R. Is weather chaotic?: Coexistence of chaos and order within a generalized lorenz model. Bull. Meteorol Soc. 2021;102(1):E148 – E158. http://dx.doi.org/10.1175/BAMS-D-19-0165.1, URL https://journals.ametsoc.org/view/journals/bams/102/1/BAMS-D-19-0165.1.xml.

[25] Saiki Y, Yorke JA. Can the flap of a butterfly's wings shift a tornado into texas—Without chaos? Atmosphere 2023;14(5):821. http://dx.doi.org/10.3390/atmos14050821, URL https://www.mdpi.com/2073-4433/14/5/821.

[26] Hoffman RN. Controlling the global weather. Bull Am Meteorol Soc 2002;83(2):241–8. http://dx.doi.org/10.1175/1520-0477(2002)083<0241:CTGW>2.3.CO;2, URL http://journals.ametsoc.org/doi/10.1175/1520-0477(2002)083<0241:CTGW>2.3.CO;2.

[27] Miyoshi T, Sun Q. Control simulation experiment with lorenz's butterfly attractor. Nonlinear Process Geophys 2022;29(1):133–9. http://dx.doi.org/10.5194/npg-29-133-2022, URL https://npg.copernicus.org/articles/29/133/2022/.

[28] Ouyang M, Tokuda K, Kotsuki S. Reducing manipulations in a control simulation experiment based on instability vectors with the lorenz-63 model. Nonlinear Process Geophys 2023;30(2):183–93. http://dx.doi.org/10.5194/npg-30-183-2023, URL https://npg.copernicus.org/articles/30/183/2023/.

[29] Kawasaki F, Kotsuki S. Leading the lorenz 63 system toward the prescribed regime by model predictive control coupled with data assimilation. Nonlinear Process Geophys 2024;31(3):319–33. http://dx.doi.org/10.5194/npg-31-319-2024, URL https://npg.copernicus.org/articles/31/319/2024/.

[30] Nagai R, Bai Y, Ogura M, Kotsuki S, Wakamiya N. Evaluation of the effectiveness of an intervention strategy in a control simulation experiment through comparison with model predictive control. Nonlinear Process Geophys 2025;32(3):281–92. http://dx.doi.org/10.5194/npg-32-281-2025, URL https://npg.copernicus.org/articles/32/281/2025/.

[31] Ott E, Grebogi C, Yorke JA. Controlling chaos. Phys Rev Lett 1990;64(11):1196–9. http://dx.doi.org/10.1103/PhysRevLett.64.1196, URL https://link.aps.org/doi/10.1103/PhysRevLett.64.1196.

[32] Grebogi C, Lai Y-C. Controlling chaotic dynamical systems. Systems Control Lett 1997;31(5):307–12. http://dx.doi.org/10.1016/S0167-6911(97)00046-7, Control of Chaos and Synchronization. URL https://www.sciencedirect.com/science/article/pii/S0167691197000467.

[33] Boccaletti S, Farini A, Kostelich EJ, Arecchi FT. Adaptive targeting of chaos. Phys Rev E 1997;55(5):R4845–8. http://dx.doi.org/10.1103/PhysRevE.55.R4845, URL https://link.aps.org/doi/10.1103/PhysRevE.55.R4845.

[34] Pyragas V, Pyragas K. Delayed feedback control of the lorenz system: An analytical treatment at a subcritical Hopf bifurcation. Phys Rev E 2006;73(3):036215. http://dx.doi.org/10.1103/PhysRevE.73.036215, URL https://link.aps.org/doi/10.1103/PhysRevE.73.036215.

[35] Postlethwaite CM, Silber M. Stabilizing unstable periodic orbits in the lorenz equations using time-delayed feedback control. Phys Rev E 2007;76(5):056214. http://dx.doi.org/10.1103/PhysRevE.76.056214, URL https://link.aps.org/doi/10.1103/PhysRevE.76.056214.

[36] Purewal AS, Krauskopf B, Postlethwaite CM. Global effects of time-delayed feedback control applied to the lorenz system. In: Schöll E, Klapp SHL, Hövel P, editors. Control of self-organizing nonlinear systems. Cham: Springer International Publishing; 2016, p. 81–103. http://dx.doi.org/10.1007/978-3-319-28028-8_5, URL https://link.springer.com/chapter/10.1007/978-3-319-28028-8_5.

[37] Yu X. Controlling lorenz chaos. Int J Syst Sci 1996;27(4):355–9. http://dx.doi.org/10.1080/00207729608929224, URL http://www.tandfonline.com/doi/abs/10.1080/00207729608929224.

[38] Yau H-T, Yan J-J. Design of sliding mode controller for lorenz chaotic system with nonlinear input. Chaos Solitons Fractals 2004;19(4):891–8. http://dx.doi.org/10.1016/S0960-0779(03)00255-8, URL https://www.sciencedirect.com/science/article/pii/S0960077903002558.

[39] Ding J, Lei Y. Control of chaos with time-delayed feedback based on deep reinforcement learning. Phys D: Nonlinear Phenom 2023;451:133767. http://dx.doi.org/10.1016/j.physd.2023.133767, URL https://www.sciencedirect.com/science/article/pii/S0167278923001215.

[40] Eckhardt B, Yao D. Local Lyapunov exponents in chaotic systems. Phys D: Nonlinear Phenom 1993;65(1–2):100–8. http://dx.doi.org/10.1016/0167-2789(93)90007-N, URL https://linkinghub.elsevier.com/retrieve/pii/016727899390007N.

[41] Guégan D, Leroux J. Local Lyapunov exponents: A new way to predict chaotic systems. In: Topics on chaotic systems - selected papers from CHAOS 2008 international conference. Chania, Crete, Greece: World Scientific; 2009, p. 158–65. http://dx.doi.org/10.1142/9789814271349_0018, URL http://www.worldscientific.com/doi/abs/10.1142/9789814271349_0018.

[42] Han Y, Ding J, Du L, Lei Y. Control and anti-control of chaos based on the moving largest Lyapunov exponent using reinforcement learning. Phys D: Nonlinear Phenom 2021;428:133068. http://dx.doi.org/10.1016/j.physd.2021.133068, URL https://www.sciencedirect.com/science/article/pii/S0167278921002256.

[43] Van Veen L. Baroclinic flow and the lorenz-84 model. Int J Bifurc Chaos 2003;13(08):2117–39. http://dx.doi.org/10.1142/S0218127403007904, URL https://www.worldscientific.com/doi/abs/10.1142/S0218127403007904.

[44] Freire JG, Bonatto C, DaCamara CC, Gallas JAC. Multistability, phase diagrams, and intransitivity in the lorenz-84 low-order atmospheric circulation model. Chaos: An Interdiscip J Nonlinear Sci 2008;18(3):033121. http://dx.doi.org/10.1063/1.2953589, URL https://pubs.aip.org/cha/article/18/3/033121/341846/Multistability-phase-diagrams-and-intransitivity.

[45] Zhu Y, Newell RE. A proposed algorithm for moisture fluxes from atmospheric rivers. Mon Weather Rev 1998;126(3):725–35. http://dx.doi.org/10.1175/1520-0493(1998)126<0725:APAFMF>2.0.CO;2, URL https://journals.ametsoc.org/view/journals/mwre/126/3/1520-0493_1998_126_0725_apafmf_2.0.co_2.xml.

[46] Newman M, Kiladis GN, Weickmann KM, Ralph FM, Sardeshmukh PD. Relative contributions of synoptic and low-frequency eddies to time-mean atmospheric moisture transport, including the role of atmospheric rivers. J Clim 2012;25(21):7341–61. http://dx.doi.org/10.1175/JCLI-D-11-00665.1, URL https://journals.ametsoc.org/view/journals/clim/25/21/jcli-d-11-00665.1.xml.

[47] Liapounoff A. Problème général de la stabilité du mouvement. Ann de la FacultÉ Des Sci de L'UniversitÉ de Toulouse Pour Les Sciences Mathématiques et Les Sci Phys 1907;9:203–474, URL https://www.numdam.org/item/AFST_1907_2_9__203_0/.

[48] Wolf A, Swift JB, Swinney HL, Vastano JA. Determining Lyapunov exponents from a time series. Phys D: Nonlinear Phenom 1985;16(3):285–317. http://dx.doi.org/10.1016/0167-2789(85)90011-9, URL https://www.sciencedirect.com/science/article/pii/0167278985900119.

[49] Haller G. Distinguished material surfaces and coherent structures in three-dimensional fluid flows. Phys D: Nonlinear Phenom 2001;149(4):248–77. http://dx.doi.org/10.1016/S0167-2789(00)00199-8, URL https://www.sciencedirect.com/science/article/pii/S0167278900001998.

[50] Nolan PJ, Serra M, Ross SD. Finite-time Lyapunov exponents in the instantaneous limit and material transport. Nonlinear Dynam 2020;100(4):3825–52. http://dx.doi.org/10.1007/s11071-020-05713-4.

[51] Lapeyre G. Characterization of finite-time Lyapunov exponents and vectors in two-dimensional turbulence. Chaos: An Interdiscip J Nonlinear Sci 2002;12(3):688–98. http://dx.doi.org/10.1063/1.1499395, URL https://pubs.aip.org/cha/article/12/3/688/447117/Characterization-of-finite-time-Lyapunov-exponents.

[52] Aurell E, Boffetta G, Crisanti A, Paladin G, Vulpiani A. Predictability in the large: an extension of the concept of Lyapunov exponent. J Phys A: Math Gen 1997;30(1):1–26. http://dx.doi.org/10.1088/0305-4470/30/1/003, URL https://iopscience.iop.org/article/10.1088/0305-4470/30/1/003.

[53] Kraft D. A software package for sequential quadratic programming. Report, DLR German Aerospace Center — Institute for Flight Mechanics; 1988.

[54] Nakazawa T, Miyoshi T, Sakajo T, Takatama K. An overview of Japan's moonshot goal 8 R&D program for controlling and modifying the weather by 2050. 2024, http://dx.doi.org/10.5194/egusphere-egu24-13655, EGU General Assembly 2024, Vienna, Austria, 14–19 Apr 2024, EGU24-13655.

[55] Miyoshi T. A duality principle for chaotic systems: from data assimilation to efficient control. Nonlinear Dynam 2026;114(2):105. http://dx.doi.org/10.1007/s11071-025-12021-2.

[56] Bodnar C, Bruinsma WP, Lucic A, Stanley M, Allen A, Brandstetter J, Garvan P, Riechert M, Weyn JA, Dong H, Gupta JK, Thambiratnam K, Archibald AT, Wu C-C, Heider E, Welling M, Turner RE, Perdikaris P. A foundation model for the earth system. Nature 2025;641(8065):1180–7. http://dx.doi.org/10.1038/s41586-025-09005-y.

[57] Lang S, Alexe M, Chantry M, Dramsch J, Pinault F, Raoult B, Clare MCA, Lessig C, Maier-Gerber M, Magnusson L, Ben Bouallègue Z, Nemesio AP, Dueben PD, Brown A, Pappenberger F, Rabier F. AIFS – ECMWF's data-driven forecasting system. 2024, URL https://arxiv.org/abs/2406.01465 arXiv:2406.01465.

[58] Bi K, Xie L, Zhang H, Chen X, Gu X, Tian Q. Accurate medium-range global weather forecasting with 3D neural networks. Nature 2023;619(7970):533–8. http://dx.doi.org/10.1038/s41586-023-06185-3.